The International Archives of the Photogrammetry, Remote Sensing and Spatial Information Sciences, Volume XLVIII-2/W8-2024
8th International ISPRS Workshop LowCost 3D - Sensors, Algorithms, Applications, 12–13 December 2024, Brescia, Italy

Research on Photogrammetric Processing Methods for Unmanned Aerial Vehicle Imagery in Antarctica

Lechen Hu[1], Yansong Duan[1,*]

[1] School of Remote Sensing and Information Engineering, Wuhan University, Wuhan 430079, China - hlc118@whu.edu.cn, ysduan@whu.edu.cn

Commission II

Keywords: Antarctica, UAV Photogrammetry, Coordinate Transformation, Image Retrieval and Matching.

Abstract

Antarctica, abundant in resources and of exceptional scientific value, is a focus of research. Unmanned aerial vehicle (UAV) photogrammetry, as a low-cost and efficient method for geographic information acquisition, plays an important role in Antarctic studies. However, due to the unique conditions of Antarctica, conventional UAV photogrammetry processing methods are inadequate, and relevant research in this area is limited. This paper uses a photogrammetric coordinate system for the Antarctic environment and derives the conversion formulas between geodetic coordinates and the coordinates. This paper also discusses methods for image matching to accelerate image retrieval speed and improve retrieval efficiency in the harsh natural conditions in Antarctica. The results of photogrammetric production using real data confirm that the proposed planar coordinate system is suitable for Antarctic image processing, and the proposed retrieval method effectively addresses the challenges in Antarctic image matching. This provides valuable insights for UAV photogrammetry research in Antarctica.

1. Introduction

Antarctic is located in a high-latitude region, covering one-tenth of the Earth's land area. The average temperature in Antarctica is $-25\,^{\circ}\mathrm{C}$, with minimum temperatures reaching as low as $-88.3\,^{\circ}\mathrm{C}$. The coastal wind speed averages $17.18\,\mathrm{m/s}$, while maximum wind speeds can reach up to $100\,\mathrm{m/s}$. For these reasons, Antarctica is often referred to as the "Coldest Place on Earth" and the "Windiest Place on Earth." Located in a unique geographical position and experiencing extreme weather conditions, Antarctica is minimally influenced by human activities, making it the last pristine land on Earth and a valuable site for various scientific explorations. And its distinctive ecological environment also serves as a focal point for global ecological research and conservation. Moreover, Antarctica possesses rich resources, including over 220 mineral resources and energy deposits, substantial reserves of iron and coal, as well as significant potential for wind, wave (or tidal), and geothermal energy resources. Antarctica also stores approximately 72% of the world's available freshwater, which could sustain the global population for 7500 years (Jiangang Zhu et al., 2006). The marine resources, mineral and energy deposits, and freshwater resources in Antarctica have enormous potential for development.

Unmanned aerial vehicles (UAVs) are pilotless aircraft equipped with propulsion devices and navigation modules, capable of reliable flight control within a specified range through remote radio control or pre-programmed autonomous control (Adam C. Watts et al., 2012). As a low-altitude remote sensing platform, UAVs have been widely used in conventional environments in recent years due to their increasing civilian and commercial applications. Utilizing UAVs for photogrammetry, with high-resolution images and POS (position and orientation system) data, enables applications such as three-dimensional modeling and dynamic monitoring, with related technologies being well-established.

In the Antarctic environment, UAVs offer advantages such as low cost, high efficiency, portability, and low risk. Compared to manned aircraft, UAVs have a smaller size, lower operational and maintenance costs, and more flexible requirements for takeoff and landing conditions. During operations, remote control can be conducted from a safe area, enhancing overall safety. The use of UAV photogrammetry allows for detailed mapping of targets, providing robust data support for studies on glacier dynamics, Antarctic topography mapping, and the selection of new research station sites. Moreover, the photogrammetric theories and methods developed for Antarctica can also be applied to studies in the Arctic and mountainous regions.

Before the popularization of UAVs, Chinese scholars had made certain attempts and explorations in the aerial photogrammetry of Antarctica (Deren Li and Xiuxiao Yuan, 1992; Shunan Gong and Shanchang Wu, 2008; Wenhui Wu et al., 2010; Min Xu et al., 2016; Hongyu Cui et al., 2005). And with the maturity of UAV technology and growing focus on Antarctic, research on the application of UAVs in Antarctica has been increasing. Those applications are mainly focused on glacier monitoring(Maciej Dąbski et al., 2017; I. V. Florinsky and D. P. Bliakharskii, 2019; D.P. Bliakharskii et al., 2019; Clare Gaffey and Anshuman Bhardwaj, 2020), topographic mapping(Maciej Dąbski et al., 2017; Teng Li et al., 2019; Baogang Zhang et al., 2019), and ecological monitoring(Arko Lucieer et al., 2014; Christian Pfeifer et al., 2019; W. Chris Oosthuizen et al., 2020; Vasco Miranda et al., 2020; Katarzyna Fudala and Robert Józef Bialik, 2022). Some scholars used satellite data, such as optical imagery, radar, and altimeter data, to obtain local or global DEM data for Antarctica using methods such as optical photogrammetry(Kaoru Shiramizu et al., 2017; Ian M. Howat et al., 2019; Michael Abrams et al., 2020), synthetic aperture radar interferometry(Birgit Wessel et al., 2021), or multi-source data integration(Yuting Dong et al., 2022). These DEM data provide strong support for polar research. Some researchers have studied the factors that may affect UAV photogrammetry operations in Antarctica. Teng Li et al. (2022) comprehensively summar-

ized the potential factors that UAVs may encounter in Antarctic scientific research, including meteorological, electromagnetic, and light reflection factors. Yang Feng et al. (2016) and Lizhong Zhu et al. (2021) summarized the problems and solutions that may arise in Antarctic UAV oblique photogrammetry.

The Antarctic is located in a high-latitude region, and commonly used projection coordinate systems, such as the Gauss-Krüger projection (Transverse Mercator) and Web Mercator projection, are not well-suited for photogrammetric work. As shown in Figure 1, Web Mercator projection (Google, n.d.-a) experiences significant distortion at the poles and cannot represent areas above 85 degrees latitude. Choosing an appropriate coordinate system is fundamental for photogrammetry, making related research necessary.

Figure 1. Google Earth uses the Web Mercator projection.

Additionally, strong winds, snow, rain, and low temperatures in Antarctica shorten UAV flight windows, often requiring multiple operations to cover the survey area. This results in irregular flight strips and unordered data distribution, which can impact current matching methods. Efficient image retrieval methods are needed to improve matching efficiency.

Despite the rapid growth in Antarctic UAV research, studies addressing the photogrammetry theories and production workflows mentioned above are relatively scarce. These are the key challenges faced in Antarctic UAV photogrammetry. To address these issues, this paper investigates data processing methods for UAV imagery in Antarctica, particularly regarding coordinate systems and image matching, aiming to produce photogrammetric outputs such as Digital Orthophoto Maps (DOMs).

2. Methods

2.1 Tangent Plane Coordinate System

Photogrammetric measurements are typically conducted using the Gauss-Krüger projection coordinate system. However, Antarctica, located in a high-latitude area, is not suitable for photogrammetric measurements using the Gauss-Krüger projection coordinate system. As latitude increases, meridians become denser, and the coverage range of Gauss projection zones shrinks. For the same-sized survey area, higher latitudes cover a larger longitudinal range, and the variation in high-latitude areas is more significant.

The tangent plane coordinate system is a local coordinate system that allows the setting of a suitable origin based on the location of the survey area to more accurately describe the area. Under the premise of accurate coordinate conversion, it describes coordinates without "projection deformation."

Therefore, when conducting photogrammetric measurements in Antarctica, the Gauss-Krüger projection coordinate system needs to be replaced by the tangent plane coordinate system. This section provides precise formulas for the conversion between geodetic coordinates and the tangent plane coordinate system.

The tangent plane coordinate system and the space rectangular coordinate system are related by a rigid-body transformation, and there is also a transformation relationship between the geodetic coordinate system and the space rectangular coordinate system. Therefore, with the help of the space rectangular coordinate system, it is possible to achieve the conversion between the geodetic coordinate system and the tangent plane coordinate system.

Based on the knowledge of ellipsoidal mathematical projection, the curvature radii of the prime vertical and the meridian at a certain point are calculated using the following formulas:

$$\begin{aligned} M &= \frac{a(1-e^2)}{W^3} \\ N &= \frac{a}{W} \\ W &= \sqrt{1-e^2\sin^2 B} \end{aligned} \tag{1}$$

where a is the semi-major axis of the ellipsoid, e is the first eccentricity of the ellipsoid, M is is the curvature radius of the meridian, N is is the curvature radius of the prime vertical, W is an auxiliary variable.

The conversion relationship from geodetic coordinates to space rectangular coordinates is shown in formulas (2):

$$\begin{aligned} X &= (N+H)\cos B\cos L \\ Y &= (N+H)\cos B\sin L \\ Z &= [N(1-e^2)+H]\sin B \end{aligned} \tag{2}$$

The reverse transformation from space rectangular coordinates to geodetic coordinates is shown in formulas (3):

$$\begin{aligned} L &= \arctan\left(\frac{Y}{X}\right) \\ B &= \arctan\left(\frac{Z+Ne^2\sin B}{\sqrt{X^2+Y^2}}\right) \\ H &= \frac{Z}{\sin B} - N(1-e^2) \end{aligned} \tag{3}$$

In formulas (2) and (3), (X, Y, Z) represents space rectangular coordinates, and (B, L, H) represents geodetic coordinates. In the calculation of B in formula (3), the right side of the equation involves B as an unknown, and N is a function of B, so an iterative method is needed for solving. A initial value for B needs to be provided for the iteration. After obtaining B through iteration, H can be calculated.

The geodetic longitude L_0 and latitude B_0 of the origin o of the tangent plane coordinate system completely determine the rotation angle of the coordinate system about the space rectangular coordinate system.

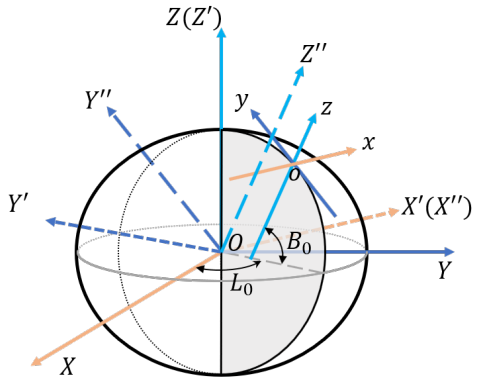

Figure 2. Rotation relationship between space rectangular coordinate system and tangent plane coordinate system.

As shown in Figure 2, the space rectangular coordinate system $O-XYZ$ first rotates about the Z-axis by $L_0+\pi/2$ to obtain $O-X'Y'Z\prime$, then rotates about X'-axis by $\pi/2-B_0$ to obtain $O-X''Y''Z''$, and finally translates to obtain the tangent plane coordinate system $o-xyz$. Therefore, the transformation formulas are as follows:

$$\begin{aligned}\begin{bmatrix}X\\Y\\Z\end{bmatrix} &= R_{z,L_0+\pi/2}R_{x,\pi/2-B_0}\begin{bmatrix}x\\y\\z\end{bmatrix}+\begin{bmatrix}X_0\\Y_0\\Z_0\end{bmatrix}\\ &= R_{et}\begin{bmatrix}x\\y\\z\end{bmatrix}+\begin{bmatrix}X_0\\Y_0\\Z_0\end{bmatrix}\end{aligned} \tag{4}$$

$$R_{et}=\begin{bmatrix}-\sin L_0 & -\cos L_0\sin B_0 & \cos L_0\cos B_0\\ \cos L_0 & -\sin L_0\sin B_0 & \sin L_0\cos B_0\\ 0 & \cos B_0 & \sin B_0\end{bmatrix} \tag{5}$$

The inverse transformation is:

$$\begin{bmatrix}x\\y\\z\end{bmatrix}=R_{et}^{\mathrm{T}}\begin{bmatrix}X-X_0\\Y-Y_0\\Z-Z_0\end{bmatrix} \tag{6}$$

where (X,Y,Z) and (x,y,z) are the space rectangular coordinates and tangent plane coordinates of a certain point, and (X_0,Y_0,Z_0) and (B_0,L_0,H_0) are the space rectangular coordinates of the origin o of the tangent plane coordinate system and the geodetic coordinates, respectively. $R_{z,L_0+\pi/2}$ is the rotation matrix about the z-axis by $L_0+\pi/2$, $R_{x,\pi/2-B_0}$ is the rotation matrix about the x-axis by $\pi/2-B_0$, and R_{et} is the rotation matrix from the tangent plane coordinates to the space rectangular coordinates.

The conversion between the geodetic coordinate system and the tangent plane coordinate system can be achieved with formulas (2), (3), (4), and (6). When converting real survey data from the geodetic coordinate system to the tangent plane coordinate system, the geodetic coordinates (B_0,L_0,H_0) of the origin o of the tangent plane coordinate system can be used as initial values. During coordinate system transformation, it is also necessary to calculate the space rectangular coordinates of the origin o of the tangent plane coordinate system using formula (2).

2.2 Under-Stable Flight Strip Image Matching

When performing matching of corresponding points in images, it is crucial to search for multiple images that may contain these corresponding points. The simplest method is to pairwise match all images, which works well when the number of images is small. However, this method is inefficient and does not make use of spatial information or organize images effectively to reduce redundant computations. As the number of images increases, the pairwise matching method becomes impractical for large-scale, small-format UAV image matching. In the case of an unstable flight strip, the adjacency of images is less correlated with the order of image acquisition, making it less suitable for exhaustive pairwise matching. Therefore, this paper adopts image matching methods based on POS and vocabulary tree to improve matching efficiency.

For images with POS data, the POS information includes the spatial relationships between images. By comparing the GPS coordinates between images, the adjacency relationship between images can be determined, facilitating image retrieval and matching. Utilizing spatial indexing methods, such as k-d trees, can expedite the retrieval process.

A k-d tree is a binary search tree used for associative retrieval. The nodes of a k-d tree represent points in k-dimensional space. Each non-leaf node can be viewed as a hyperplane dividing the k-dimensional space into two subspaces. Based on this division, other k-dimensional points are classified into two categories and assigned as the left and right subtrees of that node. By recursively partitioning the space along different dimensions until it cannot be further divided, all k-dimensional data points are organized into the nodes (including leaf nodes) of the k-d tree. This structure allows the k-d tree to quickly locate data points in k-dimensional space (Jon Louis Bentley, 1975).

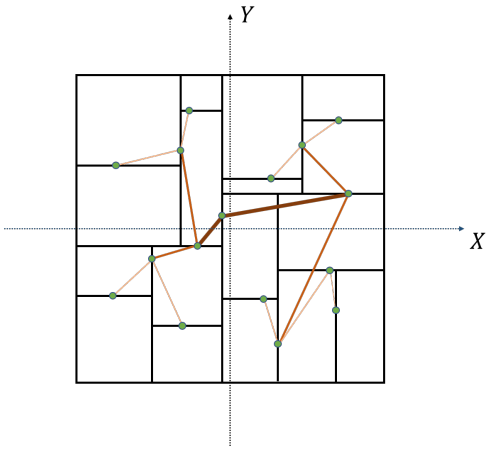

Figure 3. Illustration of a 2D k-d tree.

Once the k-d tree is constructed, the given point's adjacent points can be efficiently located using binary search and backtracking. This data structure enables rapid identification of other images adjacent to a given image, facilitating the screening of potentially matching images. In cases with a large number of images, this method effectively accomplishes the image retrieval and matching tasks.

Images lacking POS data cannot utilize k-d trees for spatial retrieval. However, since adjacent images exhibit certain similarities, image feature retrieval can be employed for finding neighboring images.

A Vocabulary Tree is a data structure used for image retrieval. For a set of image data, local features are extracted from each image, and these features are clustered, with the cluster centers referred to as "visual words." The structure of a Vocabulary Tree is a k-ary tree, named for its nodes consisting of visual words (D. Nister and H. Stewenius, 2006). Using a Vocabulary Tree, image retrieval can be transformed into a vector similarity measurement, enhancing the efficiency of image retrieval.

The construction of a Vocabulary Tree begins by obtaining all local features from each image, commonly detected and described using the SIFT algorithm (David G. Lowe, 2004). Figure 4 shows the process of obtaining all features, clustering using the k-means method, and obtaining the cluster centers as the root nodes of the Vocabulary Tree. Each cluster's features undergo another k-means clustering, resulting in k sub-cluster centers as child nodes of the current node. This clustering process is repeated until the preset depth is reached, establishing a k-ary tree, namely the Vocabulary Tree.

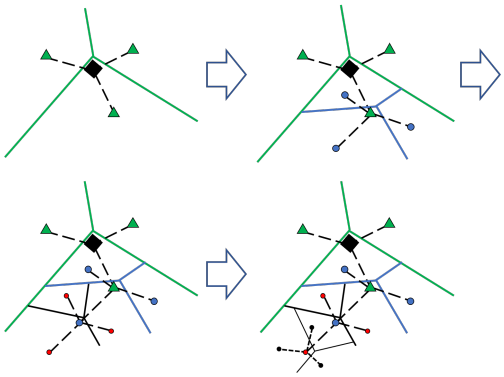

Figure 4. Construction of a k-ary vocabulary tree (k=3).

Utilizing the constructed Vocabulary Tree, an image can be transformed into a retrieval vector. Based on all local features of the image, a hierarchical k-means clustering method similar to building the Vocabulary Tree assigns these features to the leaf nodes. The leaf nodes of the Vocabulary Tree allocate different weights based on entropy, calculated using formula (7):

$$w_i = \ln \frac{N}{N_i} \tag{7}$$

Here, w_i represents the weight of the i-th leaf node, N is the number of images in the database, and N_i is the number of database images through which at least one feature passes through the i-th leaf node. Each leaf node of the Vocabulary Tree corresponds to a component of the retrieval vector, and the value of this component is determined by the frequency of features passing through the leaf node and the weight of the leaf node. The calculation formula for each component of the retrieval vector is shown in formula (8):

$$q_i = n_i w_i \tag{8}$$

Here, q_i is the i-th component of the retrieval vector, and n_i is the frequency of features passing through the i-th leaf node. Finally, the score between the retrieval vectors q of the reference image and q' of the query image determines the similarity between the two images. The score calculation formula is given in formula (9):

$$s(q, q') = \| \frac{q}{\|q\|} - \frac{q'}{\|q'\|} \| \tag{9}$$

When calculating the score, the L_1 norm often yields better results than the L_2 norm.

Organizing image features using a Vocabulary Tree enables rapid retrieval of similar images. For two similar UAV images, there is a high likelihood of overlapping regions, indicating spatial adjacency. Therefore, the Vocabulary Tree can expedite the image matching process, especially in scenarios with a large number of images and an under-stable flight strip.

3. Experiment

The image data used in this paper is from the 38th and 39th Antarctic scientific expeditions of the Chinese Antarctic expedition team. Two survey areas, denoted as Area 1 and Area 2, were captured during these expeditions. Area 1 includes the main station area of Zhongshan Station and its surrounding areas. Area 2 is a snowy area outside Zhongshan Station. Information about the two areas is shown in Table 1 and Figure 5 (Google, n.d.-b). The image data from two areas are illustrated in Figure 6.

	Area 1	Area 2
Features	Zhongshan Station and surroundings	Snowy area outside Zhongshan Station
Sub-areas	9	1
Image count	Average of 333 images	307 images
Latitude range	$-69°22'48.29''$ to $-69°21'42.21''$	$-69°37'31.83''$ to $-69°37'12.68''$
Longitude range	$76°21'21.59''$ to $76°22'49.86''$	$76°27'9.74''$ to $76°30'15.55''$
Capture time	January to March 2022	December 2022
Camera model	FC6360	EP800
Image resolution	1600×1300	5472×3648
Focal length	5.74 mm	8.8 mm
Pixel size	≈ 0.0034 mm	≈ 0.0024 mm

Table 1. Overview of survey areas and image data.

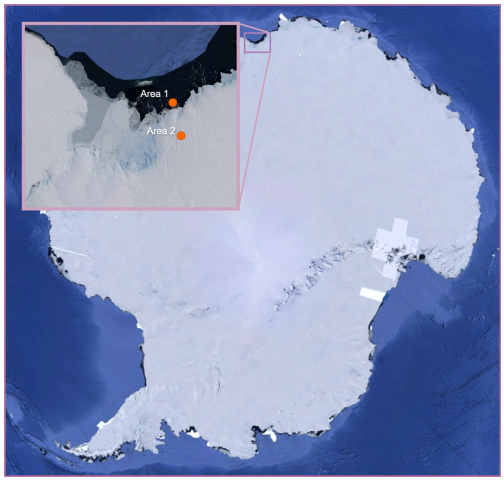

Figure 5. Locations of two areas.

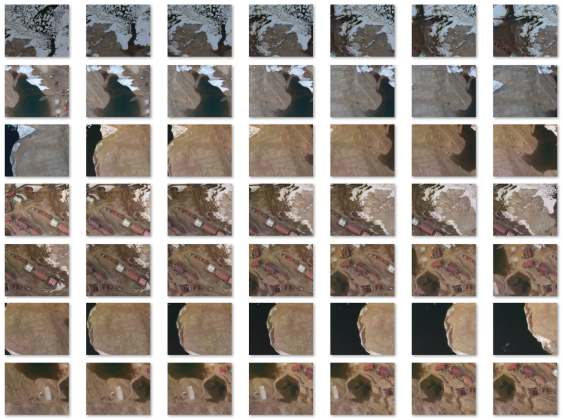

(a) Thumbnails of some images from Area 1.

(b) One image from Area 1.

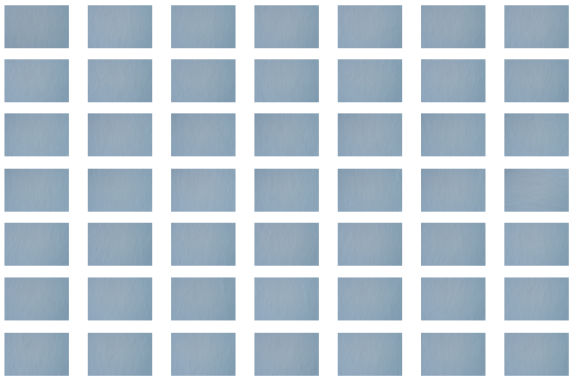

(c) Thumbnails of some images from Area 2.

(d) One image from Area 2.

Figure 6. Image data of the survey areas.

The Antarctic DEM data used in the experiment comes from the work of Yuting Dong et al. (2022), obtained through interpolation with multiple sources. The DEM uses a universal polar stereographic projection with a standard parallel circle at 71 °S and a resolution of 100m.

3.1 Coordinate Transformation

To ensure the normal progress of the subsequent image processing workflow, coordinate transformation is required. Using the EXIF data of the UAV images, extract the GPS data and gimbal attitude angle data. After extracting the POS data of the survey area, it is necessary to determine and record the origin coordinates of the local coordinate system to achieve the transformation between the geodetic coordinate system and the local coordinate system. Calculate the coordinate range of the survey area and select the center of the survey area as the origin of the local coordinate system. Use the transformation formulas (2), (5), (4), and (6) to convert GPS coordinates to local coordinates.

The geodetic coordinates of the origin of the tangent plane coordinate system for Area 1 are $(B, L, H) = (-69.3741528333, 76.3682559584, 0)$. The results of the coordinate conversion for selected points are shown in Table 2.

ID	x	y	z
116_0010	217.8338	514.7405	308.0506
116_0020	181.3597	517.7649	307.8925
116_0030	146.1324	522.9083	307.9319
116_0040	110.952	528.1225	307.9822
116_0050	75.7266	533.3269	307.8883
116_0060	40.8027	538.5245	307.9142
116_0070	5.6666	543.7186	307.9269
116_0080	-29.4193	548.9307	307.8794
116_0090	-64.5983	554.164	307.6097
116_0100	-99.6475	559.3751	307.9917

Table 2. POS data conversion results of Area 1.

3.2 Image Matching

To improve the matching efficiency of the algorithm, we employed a POS-based image retrieval method, using a k-d tree to search for nearby images as potential matches. The matching results with a search distance limited to $100\,\mathrm{m}$ in Area 1 are shown in Figure 7. From left to right, top to bottom, the spatial distance between the retrieved images and the query image increases. Since the query image is located at the junction of two flight missions, there are noticeable radiometric differences in the retrieved images. Additionally, as the images are ordered based on the distance from the capture POS, images taken at different times alternate in the results.

3.3 Bundle Adjustment

With the matched corresponding point coordinates, a system of equations can be established for bundle adjustment. Using the adjustment method, the orientation elements and ground point coordinates can be solved, and the residuals of the image point coordinates can be calculated.

For Area 1, after removing some invalid images, there are a total of 425 images in the area. According to the adjustment report, the root mean square error (RMSE) of all tie points is $6.447 \times 10^{-3}\,\mathrm{mm}$ (1.9 pixels). The maximum RMSE in the x and y directions for each individual image is $1.1177 \times 10^{-2}\,\mathrm{mm}$ (3.3 pixels) and $2.166 \times 10^{-2}\,\mathrm{mm}$ (6.4 pixels), respectively.

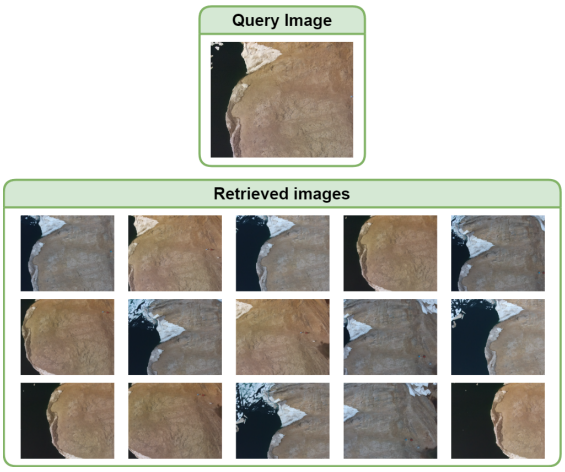

Figure 7. Image retrieval results.

For Area 2, the image quality is good, with 278 usable images remaining after removing some invalid ones. According to the adjustment report, the RMSE of all tie points is 1.006×10^{-2} mm (4.2 pixels). The maximum RMSE in the x and y directions for each individual image is 9.140×10^{-3} mm (3.8 pixels) and 9.271×10^{-3} mm (3.9 pixels), respectively.

Considering the unique conditions in Antarctica, the accuracy of the adjustment results is quite reasonable.

3.4 Production

After bundle adjustment and other procedures, DEM and DOM can be generated.

For Area 1, DEM and DOM are shown in Figure 8. Overall, the quality of the DEM and DOM is satisfactory. There is almost no fuzzy misalignment. However, in some areas with the low sidelap of the images, image connection is affected. As shown in the magnified area in the upper right corner of Figure 8a, there is some blurring such as the blurred snow near the seam line.

For Area 2, the area exhibits a stable strip pattern with uniform distribution of images. However, due to all images being captured over snowy terrain, the matching process is challenging. Utilizing the aforementioned methods results in the corresponding DEM and DOM shown in Figure 9, respectively. The terrain in the target area is generally flat, with the DEM exhibiting a gentle slope. The quality of both DEM and DOM is satisfactory. Upon zooming in, as shown in Figure 10, there is no apparent blurring or misalignment near the seam lines of the DOM, indicating a successful stitching process.

Overall, the quality of the DEM and DOM for the survey area is satisfactory, successfully completing the photogrammetric work for the area.

4. Conclusion

This paper, based on the analysis of the current status and issues of Antarctic UAV photogrammetry, proposes a feasible solution. The paper utilizes a local coordinate system to describe the target survey area and derives precise transformation formulas. Simultaneously, addressing matching issues in the Antarctic environment, the paper proposes a method to accelerate

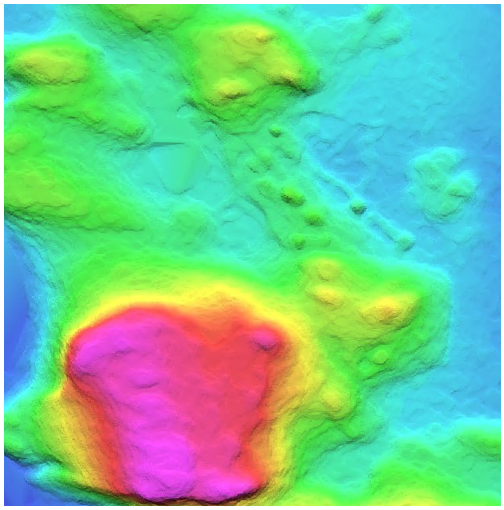

(a) The DEM of Area 1.

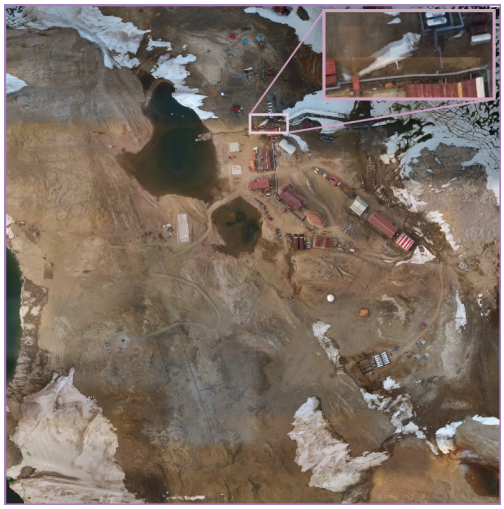

(b) The DOM of Area 1.

Figure 8. Photogrammetric products of Area 1.

(a) The DEM of Area 2.

(b) The DOM of Area 2.

Figure 9. Photogrammetric results of Area 2.

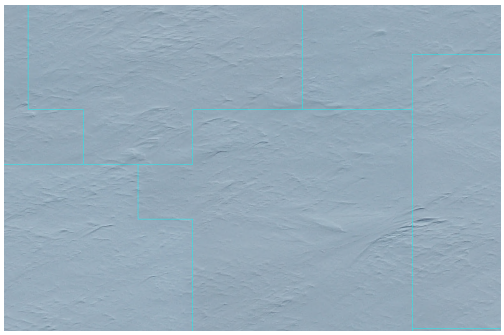

Figure 10. Local results of DOM in Area 2. The blue lines represent the stitching lines.

adjacent image retrieval using k-d trees and vocabulary trees. Experimental results with real Antarctic data demonstrate that the necessity of the tangent plane coordinate system and confirm the effectiveness of the image retrieval matching method in Antarctic UAV photogrammetry.

While this study addresses some fundamental issues in Antarctic photogrammetry, limitations remain in terms of computational efficiency, matching accuracy, adaptive parameters, and precision assessment. Future research will focus on optimizing transformation formulas, developing matching methods with higher information utilization rates, automatic parameter selection, and more reliable precision assessment methods.

Acknowledgements

This study was supported by National Key Research and Development Program of China, No. 2023YFB3905704 .

References

Adam C. Watts, Vincent G. Ambrosia, Everett A. Hinkley, 2012. Unmanned Aircraft Systems in Remote Sensing and Scientific Research: Classification and Considerations of Use. *Remote Sensing*, 4(6), 1671–1692.

Arko Lucieer, Darren Turner, Diana H. King, Sharon A. Robinson, 2014. Using an Unmanned Aerial Vehicle (UAV) to Capture Micro-Topography of Antarctic Moss Beds. *International Journal of Applied Earth Observation and Geoinformation*, 27, 53–62.

Baogang Zhang, Jian Zhao, Chi Ma, Teng Li, Xiao Cheng, Leibao Liu, 2019. Monitoring Antarctic Glacier Surface Pits Based on Unmanned Aerial Vehicle Remote Sensing Technology. *Journal of Beijing Normal University (Natural Science)*, 55(1), 19–24.

Birgit Wessel, Martin Huber, Christian Wohlfart, Adina Bertram, Nicole Osterkamp, Ursula Marschalk, Astrid Gruber, Felix Reuß, Sahra Abdullahi, Isabel Georg, Achim Roth, 2021. TanDEM-X PolarDEM 90 m of Antarctica: Generation and Error Characterization. *The Cryosphere*, 15(11), 5241–5260.

Christian Pfeifer, Andres Barbosa, Osama Mustafa, Hans-Ulrich Peter, Marie-Charlott Rümmler, Alexander Brenning, 2019. Using Fixed-Wing UAV for Detecting and Mapping the Distribution and Abundance of Penguins on the South Shetlands Islands, Antarctica. *Drones*, 3(2), 39.

Clare Gaffey, Anshuman Bhardwaj, 2020. Applications of Unmanned Aerial Vehicles in Cryosphere: Latest Advances and Prospects. *Remote Sensing*, 12(6), 948.

D. Nister, H. Stewenius, 2006. Scalable recognition with a vocabulary tree. *2006 IEEE Computer Society Conference on Computer Vision and Pattern Recognition - Volume 2 (CVPR'06)*, 2, IEEE, New York, NY, USA, 2161–2168.

David G. Lowe, 2004. Distinctive Image Features from Scale-Invariant Keypoints. *International Journal of Computer Vision*, 60(2), 91–110.

Deren Li, Xiuxiao Yuan, 1992. Bundle Adjustment of Small- and Medium-Scale Aerial Photographs in Antarctic Surveying. *Polar Research*, 27–35.

D.P. Bliakharskii, I.V. Florinsky, T.N. Skrypitsyna, 2019. Modelling Glacier Topography in Antarctica Using Unmanned Aerial Survey: Assessment of Opportunities. *International Journal of Remote Sensing*, 40(7), 2517–2541.

Google, n.d.-a. [google earth using web mercator]. Retrieved October 16, 2024, from `http://mt2.google.com/vt/lyrs=s&hl=zh-hk&g0=hk&x=0&y=0&z=0`.

Google, n.d.-b. [locations of two survey areas at the south pole station on google earth]. Retrieved October 16, 2024, from `https://earth.google.com/web/@-86.93800678,70.42264641,4371.90985357a,7854170.53897619d,35y,5.13899329h,0t,0r`.

Hongyu Cui, Wei Sun, Yanbin Niu, Kan Liu, 2005. Feasibility Study on Aerial Photogrammetry in Antarctica Using Airship. *Journal of Geomatics and Spatial Information Technology*, 6–9.

I. V. Florinsky, D. P. Bliakharskii, 2019. The 2017 Catastrophic Subsidence in the Dålk Glacier, East Antarctica: Unmanned Aerial Survey and Terrain Modelling. *Remote Sensing Letters*, 10(4), 333–342.

Ian M. Howat, Claire Porter, Benjamin E. Smith, Myoung-Jong Noh, Paul Morin, 2019. The Reference Elevation Model of Antarctica. *The Cryosphere*, 13(2), 665–674.

Jiangang Zhu, Qide Yan, Xiaoliang Ling, 2006. Antarctic Resource Disputes and Corresponding Strategies of China. *Polar Research*, 215–221.

Jon Louis Bentley, 1975. Multidimensional Binary Search Trees Used for Associative Searching. *Communications of the ACM*, 18(9), 509–517.

Kaoru Shiramizu, Koichiro Doi, Yuichi Aoyama, 2017. Generation of a High-Accuracy Regional DEM Based on ALOS/PRISM Imagery of East Antarctica. *Polar Science*, 14, 30–38.

Katarzyna Fudala, Robert Józef Bialik, 2022. The Use of Drone-Based Aerial Photogrammetry in Population Monitoring of Southern Giant Petrels in ASMA 1, King George Island, Maritime Antarctica. *Global Ecology and Conservation*, 33, e01990.

Lizhong Zhu, Zhaohui Liu, Boyu Yang, 2021. Key Issues in the Application of Drone Photogrammetry Technology in Three-Dimensional Modeling of Antarctica. *Geomatics and Spatial Information Technology*, 44(S1), 187–191.

Maciej Dąbski, Anna Zmarz, Piotr Pabjanek, Małgorzata Korczak-Abshire, Izabela Karsznia, Katarzyna J. Chwedorzewska, 2017. UAV-Based Detection and Spatial Analyses of Periglacial Landforms on Demay Point (King George Island, South Shetland Islands, Antarctica). *Geomorphology*, 290, 29–38.

Michael Abrams, Robert Crippen, Hiroyuki Fujisada, 2020. ASTER Global Digital Elevation Model (GDEM) and ASTER Global Water Body Dataset (ASTWBD). *Remote Sensing*, 12(7), 1156.

Min Xu, Qifeng Chu, Jun Yang, Rujin Yuan, Liang Zhou, 2016. Key Technologies and Related Issues in Mapping 1:5000 Topographic Maps in Antarctica—A Case Study of the Victoria Land Station. *Surveying and Mapping Engineering*, 25(1), 73–76.

Shunan Gong, Shanchang Wu, 2008. Application of Non-metric Digital Camera (Hasselblad H1D) in Antarctic Project Production. *Journal of Geomatics and Spatial Information Technology*, 162–164.

Teng Li, Baogang Zhang, Xiao Cheng, Matthew J. Westoby, Zhenhong Li, Chi Ma, Fengming Hui, Mohammed Shokr, Yan Liu, Zhuoqi Chen, Mengxi Zhai, Xinqing Li, 2019. Resolving Fine-Scale Surface Features on Polar Sea Ice: A First Assessment of UAS Photogrammetry Without Ground Control. *Remote Sensing*, 11(7), 784.

Teng Li, Baogang Zhang, Xiao Cheng, Yuanyuan Zhang, Fengming Hui, Tiancheng Zhao, Weijia Qin, Jianhong Liang, Yuande Yang, Xuying Liu, Xinqing Li, 2022. Application of Drones in Antarctic Scientific Research: Progress and Prospects. *Journal of Wuhan University (Information Science Edition)*, 47(5), 651–664.

Vasco Miranda, Pedro Pina, Sandra Heleno, Gonçalo Vieira, Carla Mora, Carlos E.G.R. Schaefer, 2020. Monitoring Recent Changes of Vegetation in Fildes Peninsula (King George Island, Antarctica) through Satellite Imagery Guided by UAV Surveys. *Science of The Total Environment*, 704, 135295.

W. Chris Oosthuizen, Lucas Krüger, William Jouanneau, Andrew D. Lowther, 2020. Unmanned Aerial Vehicle (UAV) Survey of the Antarctic Shag (Leucocarbo Bransfieldensis) Breeding Colony at Harmony Point, Nelson Island, South Shetland Islands. *Polar Biology*, 43(2), 187–191.

Wenhui Wu, Fuzhong Yin, Di Wu, 2010. Research on Aerial Photogrammetric Techniques in Antarctica Based on Helicopter Platforms and Non-metric Digital Cameras. *Polar Research*, 22(2), 190–198.

Yang Feng, Lin Qu, Jinggang Tang, 2016. Research on Assurance Methods for the Application of Oblique Photography UAV in Polar Regions. *Journal of Geomatics and Spatial Information Technology*, 39(12), 192-193+197.

Yuting Dong, Ji Zhao, Caiyong Li, Mingsheng Liao, 2022. Gapless-REMA100: A Gapless 100-m Reference Elevation Model of Antarctica with Voids Filled by Multi-Source DEMs. *ISPRS Journal of Photogrammetry and Remote Sensing*, 186, 70–82.